Electronic properties of UX_3 (X=Ga, Al, and Sn) compounds in high magnetic fields: Transport, specific heat, magnetization, and quantum oscillations

A. L. Cornelius, A. J. Arko, J. L. Sarrao, J. D. Thompson, M. F. Hundley, and C. H. Booth
Materials Science and Technology Division, Los Alamos National Laboratory, Los Alamos, New Mexico, 87545

N. Harrison
National High Magnetic Field Laboratory, Los Alamos National Laboratory, Los Alamos, New Mexico 87545

P. M. Oppeneer
Institute of Theoretical Physics, University of Technology, D-01062 Dresden, Germany
(Received 2 October 1998)

We have performed measurements of the specific heat and resistivity in static magnetic fields up to 12 T, as well as magnetic measurements in a static field of 0.1 T and in pulsed fields up to 50 T on high-quality UX_3 (X=Ga, Al, and Sn) single crystals. The behavior of the electronic specific heat coefficients in applied field $\gamma(B)$ either remains nearly constant or increases as B increases and is inconsistent with the expectations of the single-impurity model. For UGa_3, different de Haas–van Alphen (dHvA) frequencies are observed above and below a magnetic transition at a field $B_M \sim 12$ T at $T \sim 0.5$ K, indicating that a major reconstruction of the Fermi surface occurs. Neither USn_3 nor UAl_3 exhibited a magnetic transition in fields to 50 T, and only a single weak dHvA frequency was observed in these compounds. The difference between the behavior of the UX_3 compounds can be attributed to the degree of hybridization of the $5f$ orbitals with the conduction electron orbitals. UGa_3 behaves as an itinerant $5f$-electron system, while UAl_3 has a tendency to localization, but is still relatively delocalized. USn_3 is a heavy fermion compound. Concurrent to our experimental investigations we have performed calculations of the energy band structures of the three compounds. Owing to the delocalized $5f$ behavior of UGa_3, and also of UAl_3, we find that an itinerant, energy band approach explains the dHvA frequencies of antiferromagnetic UGa_3 and paramagnetic UAl_3 reasonably well. For UGa_3 an unusual sensitivity of the magnetic moment to the magnetic structure and the lattice parameter occurs, providing evidence that UGa_3 is an unique example of an itinerant uranium-based antiferromagnet. [S0163-1829(99)04321-0]

I. INTRODUCTION

The uranium compounds UX_3, where X is a IIIA or IVA element, Ru, or Rh, crystallize in the cubic $AuCu_3$-type structure with a U-U separation $d_{\text{U-U}}$ between 4.0–4.3 Å.[1] This value of $d_{\text{U-U}}$ is much larger than the Hill limit for uranium compounds,[2] and using the Hill criterion, one might naively expect magnetic ordering in all of the mentioned UX_3 compounds. Instead, they display a wide range of behavior: Pauli enhanced paramagnetism (UAl_3, USi_3, UGe_3, and URh_3), antiferromagnetism (UPb_3, UGa_3, UTl_3, and UIn_3), heavy fermion behavior (USn_3), and superconductivity (URu_3).[1,3,4] The different behaviors can be explained by the great variation in the f-electron hybridization with the X atom s, p, and d orbitals.[3] The effect of the different hybridization strengths becomes apparent in the electronic specific heat coefficient γ which varies from 14 mJ/mole K^2 in USi_3 to 171 mJ/mole K^2 in USn_3.[1,5,6]

Due to the cubic crystal structure, the wide range of hybridization strengths, and the availability of high-quality single crystals, the UX_3 compounds are excellent for examining how the measured physical properties and underlying electronic structure are interrelated. To determine these interrelations, we have measured resistivity and specific heat in static fields as high as 12 T, and magnetization in pulsed magnetic fields to 50 T on samples of UGa_3, UAl_3, and USn_3. From the measurements of the specific heat in high fields and the de Haas–van Alphen (dHvA) effect, we gain a great deal of insight into the physics of uranium compounds. For UGa_3, which has a magnetic transition at a field B_M of about 12 T at 0.47 K, the measured dHvA frequencies are different above and below B_M indicating a major reconstruction of the Fermi surface has occurred. This transition, however, displays no, or at best a very small, anomaly in the magnetization and magnetoresistance, which is quite exceptional. For the time being, the exact nature of the transition is unclear, though we hypothesize that it is due to a change in antiferromagnetic structure. For UAl_3 and USn_3 no magnetic transition was observed for fields less than 50 T at $T \approx 0.5$ K and only a single weak dHvA frequency could be detected in both compounds. The results on USn_3 should in general be explained by theories relevant to spin-fluctuation systems (see, e.g., Ref. 7), though there are some discrepancies. One fingerprint of spin fluctuations is an upturn in the specific heat C/T at low temperatures. In an early study such an upturn was observed below 3.5 K,[5] but later studies could not confirm this.[8,9] The temperature dependence of the resistivity, on the other hand, contains a T^2 term,[10] which indicates spin-fluctuation effects. Some vague indications of spin-spin correlation effects could also be deduced from

neutron-scattering experiments.[11] UAl_3, though not a heavy fermion compound, has been categorized also as a spin-fluctuating system.[12] An upturn in C/T has, however, not been reported, but our specific heat data are consistent with UAl_3 being a spin-fluctuating system. As the appropriate model to classify USn_3 and UAl_3 is one of the current questions, we shall consider also the validity of the single-impurity model to describe these compounds, next to the spin-fluctuation model. UGa_3 does not behave as a typical spin fluctuator, but rather the large hybridization leads to a stable, itinerant $5f$-electron antiferromagnet, as evidenced by numerous different measurement techniques. Our band structure calculations establish the itinerant picture of UGa_3 further. Within the itinerant f-electron approach, an overall reasonable explanation of the measured dHvA properties in the antiferromagnetic structure is attained. The itinerant $5f$-electron approach also provides an explanation for our measured dHvA data of UAl_3. The nature of the $5f$'s in UAl_3 has not yet been thoroughly investigated; one of the aims of the present study is to determine its proper classification. Our investigation points to a relatively delocalized $5f$ behavior at low temperatures.

II. EXPERIMENTAL TECHNIQUES

Single crystals of UX_3 (X=Ga, Al, and Sn) were grown using a standard flux technique,[13] with excess X used as the flux in each case. The starting constituents ($\sim$5 mol % U in excess X) were placed in an alumina crucible and sealed in an evacuated quartz ampoule. After the ampoules were slowly cooled through an appropriate temperature cycle, they were removed from the furnace at a temperature where the excess X was still molten, allowing the excess flux to be spun off using a centrifuge. The resulting well-separated single crystals were typically cubes of a few mm on a side.

A standard four-point measurement was used to measure the resistance at temperatures in the range from 0.3 to 325 K. A thermal relaxation method was used to measure the specific heat of small ($\sim$10–40 mg) samples in the temperature range from 1.3–20 K in a standard superconducting magnet capable of producing static magnetic fields as large as 12 T. The magnetization was measured in a Quantum Design SQUID magnetometer with an applied field of 0.1 T and temperatures ranging from 2 to 350 K. Also, the magnetization and dHvA effect were measured with counterwound, highly compensated pickup coils in pulsed magnetic fields up to 50 T at the National High Magnetic Field Laboratory in Los Alamos; the sample was in a ^{3}He environment and the temperature was varied between 0.47 and 3.5 K.

III. RESULTS AND DISCUSSION

A. Experiment

From our x-ray diffraction results, it was determined that all of the samples crystallized in the $AuCu_3$-type structure with cubic lattice parameters of 4.607, 4.260, and 4.264 Å for USn_3, UGa_3, and UAl_3, respectively, in good agreement with the literature values.[3] It is interesting to note that the lattice constant of UGa_3 is less than that of UAl_3. It would be expected that the lattice would expand as one moves down a column in the Periodic Table as is seen in the IVA series where UGe_3 has a lattice parameter that is 0.17 Å larger than USi_3. We attribute the anomalous behavior of the lattice parameter in UGa_3 relative to UAl_3 as being due to the much larger hybridization in UGa_3 causing the formation of $5f$ bands which lower the U-U spacing.

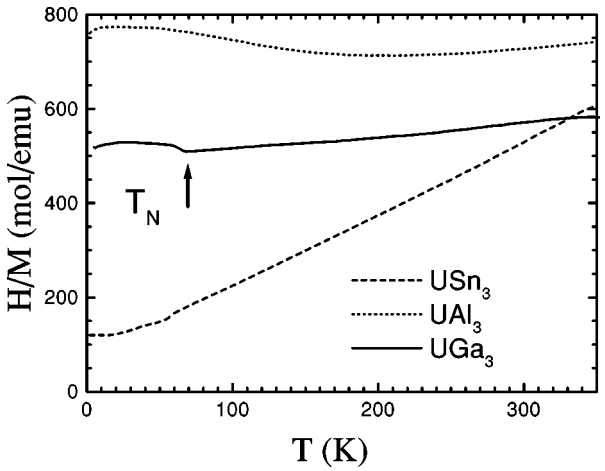

FIG. 1. The measured value of H/M at a field of 0.1 T for UGa_3, UAl_3, and USn_3. The onset of antiferromagnetic order in UGa_3 at $T=T_N$ is identified by the arrow.

The measured inverse susceptibility (the value of H/M in an applied field of 0.1 T) versus temperature for UGa_3, UAl_3, and USn_3 is shown in Fig. 1. There is clearly a rise in H/M at $T_N=68$ K for UGa_3 that corresponds to the onset of antiferromagnetic order; for $T>T_N$, there is no evidence for Curie-Weiss behavior (this has been shown to hold up to 900 K by Murasik *et al.*[14]) which has been explained by the itinerant nature of the $5f$ electrons.[15] This itinerant view of the $5f$ electrons is also supported by the pressure dependence of T_N.[16,17] From neutron diffraction and μSR experiments, the magnetic structure has been shown to consist of spins that are ferromagnetically aligned in (111) planes with adjacent (111) planes being antiferromagnetically coupled.[18,19] While the direction of the magnetic moments is not yet known unambiguously, there are experimental indications that the moments are in the (001) direction.[20] We shall come back to this point when discussing our calculations. The total moment of UGa_3 is $\sim 0.9\mu_B$/U.[18] USn_3 displays behavior typical of a moderate heavy fermion system.[21] For $T>20$ K, USn_3 exhibits Curie-Weiss behavior with $\mu_{\text{eff}}=2.29\mu_B$/U and $\Theta_p=47$ K, while at low temperatures the magnetization takes on a constant value after going through a maximum. UAl_3 displays a maximum in the measured susceptibility at $\sim$200 K, and from a previous report, Curie-Weiss behavior is seen from 240–800 K.[12] Neither USn_3 nor UAl_3 shows magnetic ordering down to 1.5 K.

The measured resistivities for the UX_3 samples are shown in Fig. 2. The values of the residual resistivity ratio $RRR \equiv \rho(295K)/\rho(4\ \text{K})$ are 49, 38, and 37 for USn_3, UGa_3, and UAl_3, respectively. The resistivity ratio for UGa_3 is much higher than previously reported values 1.7 and 11.[4,16] For UGa_3, there is a kink in the resistivity at 68 K, as shown by the arrow in Fig. 2, corresponding to the Néel temperature T_N determined from magnetization measurements shown in Fig. 1. At low temperatures, both USn_3 and UAl_3 display

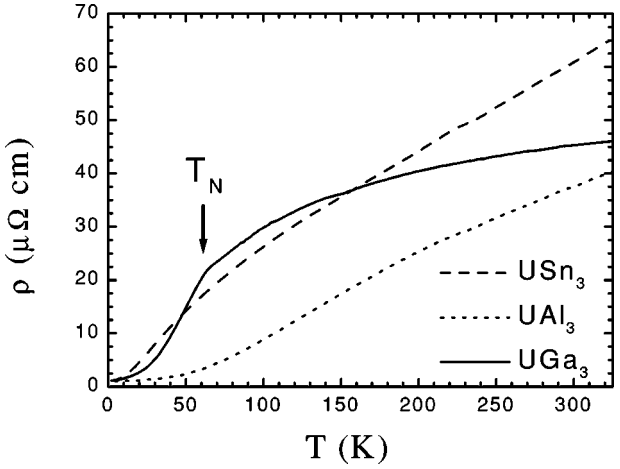

FIG. 2. The measured resistivities for USn_3, UGa_3, and UAl_3. The antiferromagnetic transition at $T_N=64$ K in UGa_3 is identified by the arrow.

resistivity that is proportional to AT^2 with a value of A that is much larger than for typical Fermi liquids. This large value of A is typical for a spin-fluctuating system and is consistent with classifying UAl_3 and USn_3 as spin fluctuators.[22,23] For USn_3, however, from both susceptibility and resistivity measurements, a small percentage ($\sim$5 vol %) of the sample displays superconductivity below 3.7 K which can be explained by the existence of Sn inclusions. Neither UAl_3 nor UGa_3 displayed traces of superconductivity down to 300 mK (the values of T_c for flux inclusions would be 1.2 K for Al in UAl_3 and 1.1 K for Ga in UGa_3). The magnetoresistance, determined at $T=1.7$ is displayed in Fig. 3 and does not saturate up to $B=10$ T for any of the three compounds. When the data is fitted to the formula

$$\frac{\rho(B)-\rho(0)}{\rho(0)} \propto B^n \tag{1}$$

in the range 3 T$<B<$10 T, we find from least squares fits, $n=0.94$ for USn_3, 2.04 for UGa_3, and 1.83 for UAl_3 with uncertainties determined from the fits on the order of 1%. We have extended the measurement to $B=50$ T at $T=0.5$ K on UGa_3 (not shown) and found that the quadratic

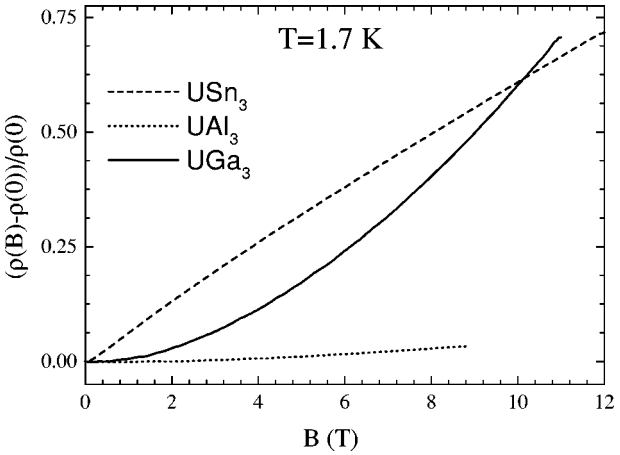

FIG. 3. The magnetoresistance versus applied magnetic field at $T=1.7$ K for USn_3, UGa_3, and UAl_3.

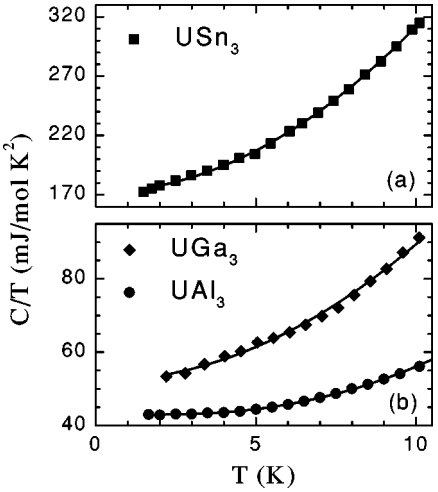

FIG. 4. The measured zero-field heat capacities for (a) USn_3 and (b) UGa_3 and UAl_3. The lines are fits to the data as described in the text.

behavior extends over the entire field range with no observed anomalies. The implications of the magnetoresistance measurements on the Fermi surface will be discussed further when we examine the results of our band structure calculations.

The zero-field data from specific heat measurements are shown in Fig. 4 (note that the values for USn_3 have been corrected for the amount of Sn inclusions in the sample). The lines represent fits to the data using

$$C/T=\gamma+\beta^*T^2+\delta T^2 \ln T, \tag{2}$$

where γ is the linear temperature electronic specific heat coefficient and β^* is given by

$$\beta^*=\beta+\beta_{\mathrm{mag}}-\delta \ln T_{sf} \tag{3}$$

and is the sum of the Debye term β, the antiferromagnetic magnon term β_{mag} (which is zero except for antiferromagnetically ordered systems), and δ and T_{sf} are due to spin-fluctuation effects. Also, β can be related to the Debye temperature Θ_D by the relation

$$\Theta_D=\left(\frac{1.944\times 10^6 \ r}{\beta}\right)^{1/3}, \tag{4}$$

where r is the number of atoms per unit cell and β is in units of mJ/mol K^4. The data were fit to Eq. (2) from 1.5 to 11 K. The data for USn_3 is shown in Fig. 4(a) and could be fit well without a spin-fluctuation term. This is similar to the result of Norman *et al.*[9] who were able to fit the data both to a Debye and a spin-fluctuating form. Measurements to lower temperatures are needed to positively conclude if the specific heat of USn_3 behaves as a spin fluctuator. The data for UGa_3 and UAl_3 are shown in Fig. 4(b). UGa_3 is fit well without the inclusion of spin-fluctuation effects. The same is not true for UAl_3 and the fit shown in Fig. 4(b) takes into account the spin-fluctuation terms. This is consistent with the results on $U_{0.5}Th_{0.5}Al_3$ where a clear minimum is seen in a plot of C/T versus T^2 which is a clear signature of a spin-fluctuation system.[24] It should be mentioned, however, that this compounds crystallizes in the noncubic DO19 structure in con-

TABLE I. Physical properties from zero-field specific heat measurements on UGa_3, USn_3, and UAl_3.

Compound	γ (mJ/mol K^2)	β^* (mJ/mol K^4)	Θ_D (K)
UGa_3	52.0±0.2	0.342	
USn_3	171.9±0.5	1.403	177
UAl_3	43.2±0.1	−0.126	–

trast to the UX_3 compounds. All of the parameters determined from the current specific heat measurements are displayed in Table I and agree well with the values of γ and Θ_D given in previous reports.[1,5,6] The error bars given for γ are simply statistical values from the least square fits. The actual experimental uncertainty is in the 1–3 % range. Also, it should be noted that γ was determined for temperatures above 1.5 K and that deviations from our reported values may occur at lower temperatures.

Though we have obtained evidence for the applicability of a spin-fluctuation model to UAl_3, and to a lesser extent on USn_3, we will also test a single-impurity model on our susceptibility and specific heat data. The results on USn_3, and also UAl_3, are consistent with the Coqblin-Schrieffer model for a single-impurity with total angular momentum J dissolved in conduction electrons, where one expects a maximum in the susceptibility[25] that is directly related to a characteristic temperature T_0 which in turn is related to the hybridization. Using the results of Rajan,[25] we find the best fits to our susceptibility data using $J=3/2$ and $T_0=61$ K for USn_3 and $J=5/2$ and $T_0=830$ K for UAl_3. Using the same parameters, the theory predicts values for γ of 27 mJ/mol K^2 for UAl_3 and 210 mJ/mol K^2 for USn_3. These values are in reasonable agreement with the measured values in Table I. From these results, one could conclude that USn_3, and also UAl_3 are strongly correlated Kondo-lattice systems with the hybridization stronger in UAl_3 ($T_0=830$ K) than in USn_3 ($T_0=61$ K). In UGa_3, the hybridization is of sufficient strength for the $5f$ electrons to be considered itinerant and to make UGa_3 behave in a similar manner to transition metal compounds. One might think that the value of γ for UGa_3, which is larger than that for UAl_3, is somewhat anomalous. However, this can once again be explained by the different degree of hybridization of the $5f$ orbitals with the conduction electron orbitals, which may for UGa_3 lead to a significant contribution of itinerant $5f$ electrons located at the Fermi energy E_F to the density-of-states $N(E_F)$ and therefore to γ.

Application of magnetic fields to heavy fermion systems can lead to dramatic effects in the measured specific heat, with the value of $\gamma(B)$ tending to decrease with applied field.[21,26] This has been explained in the single-impurity model by the broadening of the Kondo resonance with applied field.[26] It can be shown that $\gamma(B)$ in the single-impurity model may be written as

$$\gamma(B)=\left[\left(\frac{N-1}{2\gamma_0}\right)^2+\left(\frac{3\mu B}{\pi k_B R}\right)^2\right]^{-1/2}, \qquad (5)$$

where γ_0 is the zero-field value of $\gamma(B)$, N is the degeneracy, μ is an effective magnetic moment, and R is the gas constant.[27] This expression has been successfully used to explain the observed $\gamma(B)$ behavior in numerous Ce and U compounds.[26–28] Extending the analysis to the lattice case via the Anderson lattice model yields qualitatively similar results.[29] There are, however, systems which do not obey Eq. (5). For example, in systems for fields below a metamagnetic transition field B_M, it has been shown experimentally on $CeCu_2Si_2$,[30] CeB_6,[31] and UPt_3 (Ref. 32) and theoretically[33] that $\gamma(B)$ can increase for $B<B_M$ but then decrease for $B>B_M$ according to Eq. (5). Also, other compounds, such as UAu_3 (Ref. 34) and CePtSi (Ref. 35) show almost no variation of $\gamma(B)$ with applied field: this behavior could be explained by a metamagnetic transition occurring at a field B_M higher than the field range employed in the specific heat measurements. However, it is also possible that there are contributions to the specific heat that are not electronic that enhance measured γ values. These enhancements, such as magnetic correlations, can increase with applied field making γ appear to increase, though the actual behavior of γ is masked by the added contributions. It is impossible to determine the purely electronic ($\gamma \propto m^*$) contribution if these other effects are not negligible.[36]

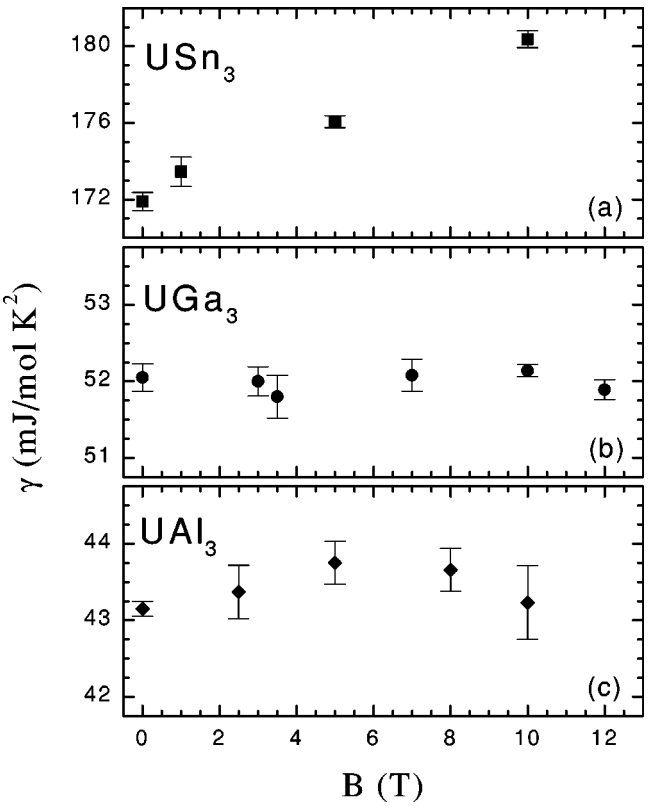

FIG. 5. The measured electronic coefficients of specific heat for USn_3, UGa_3, and UAl_3 as a function of the applied magnetic field.

The measured values of $\gamma(B)$ for USn_3, UGa_3, and UAl_3 of the current study are displayed in Fig. 5. Also, the measured values of $\beta^*(B)$ (not shown) do not change within the experimental uncertainty for any of the measured compounds. For UGa_3 and UAl_3, the measured $\gamma(B)$ does not change within the experimental uncertainty in fields to 12 T. This would be consistent with the results on other systems for fields below a metamagnetic transition, but is also what one expects from an itinerant, transition metallike compound where magnetic field has only a small effect on the density of

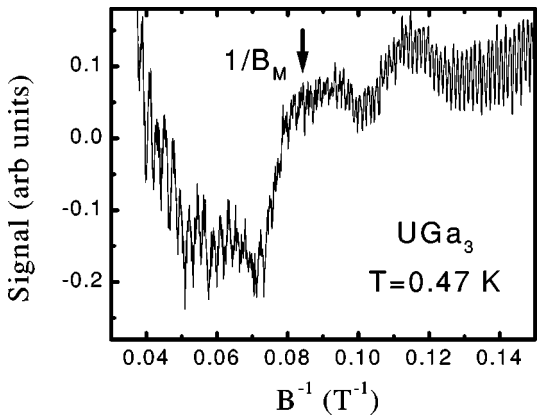

FIG. 6. The measured signal (induced voltage) versus inverse applied field B^{-1} for UGa_3 at $T=0.47$ K. There is a jump in the data at the magnetic transition at B_M. de Haas–van Alphen oscillations are clearly visible, with a different frequency spectrum above and below B_M.

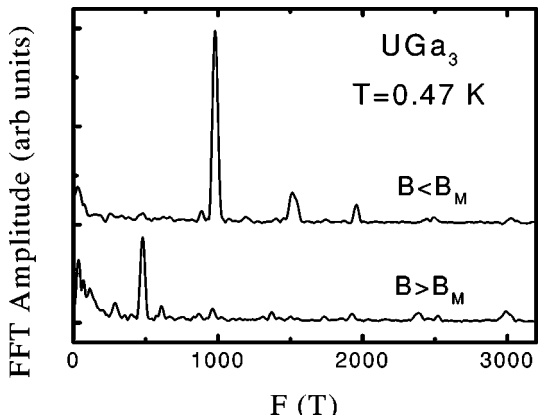

FIG. 7. The calculated fast Fourier transform of the de Haas–van Alphen data both above and below B_M for UGa_3.

states. However, most compounds which undergo a metamagnetic transition exhibit a peak in $\gamma(B)$ at B_M which is not seen in the current study on UGa_3, and as will be discussed later, the magnetization is inconsistent with the occurrence of a metamagnetic transition in UGa_3. The results for USn_3 are somewhat anomalous as we find that $\gamma(B)$ increases with applied field, but USn_3 does not exhibit an observable magnetic transition in fields up to 50 T. Thus, if USn_3 does not have a metamagnetic transition at a field higher than 50 T, it is impossible to reconcile the specific heat measurements in applied fields with the single-impurity or Anderson lattice models unless other components to the specific heat besides electronic contributions are not negligible and need to be accounted for. Further measurements of $\gamma(B)$ and the magnetization to higher fields and lower temperatures than reached in the current study would be useful to understand the $\gamma(B)$ behavior.

Measurements of the dHvA effect are the most precise experimental probes of the Fermi surface in metals. In a pulsed magnetic field, it can be shown[31] that the temperature and magnetic field dependence of the dHvA signal S is given by

$$S(B,T) \propto \left(\frac{F^2 T}{B^{5/2}}\right)\left(\frac{\partial B}{\partial t}\right)\frac{\exp[14.7 m^* T_D/B]}{\sinh[14.7 m^* T/B]}, \qquad (6)$$

where F is the frequency of the Fermi surface piece in question, B is the magnetic field in units of T, t is the time, T_D is the Dingle temperature, and m^* is the effective mass (in units of m_e the free electron mass). An examination of Eq. (6) reveals the difficulty in detecting dHvA oscillations in heavy fermion materials as the value of m^*, which strongly reduces S as m^* increases, can be very large (values of m^* as high as $110 m_e$ in UPt_3 have been observed[37]). It is important to note that the value of m^* has been observed to scale with $\gamma(B)$ as determined by dHvA and specific heat measurements on the same compound.[31,38,39] As previously mentioned, $\gamma(B)$ tends to decrease with increasing field, making the reduction in dHvA signal smaller than if the masses remained constant. However, as seen in Fig. 5, the samples of the current study have values of $\gamma(B)$ that either remain constant or increase with increasing field, which would make the dHvA signal even more difficult to detect.

All of the dHvA measurements were performed on single crystals that were roughly cubes of ~ 0.6 mm on a side with the magnetic field applied along the (100) direction. The raw magnetization data for UGa_3 at 0.47 K is displayed in Fig. 6. As can be seen, there is clearly an oscillatory dHvA signature in the data. There is a jump in the signal at B_M corresponding to the magnetic transition. It is also apparent that there is a significant change in the frequencies of the dHvA data above and below B_M. The fast Fourier transform (FFT) of the measured data for falling fields on UGa_3 is shown in Fig. 7. The value of B_M is in the range of 12–14 T for the temperatures that were measured (0.47 K$<T<$3.5 K). For $B<B_M$ (5 T$<B<$10 T) three frequencies were detected, though there may be higher mass branches of the Fermi surface that we could not detect in this relatively low field range where our sensitivity to pieces of Fermi surface with large masses is rather poor. A summary of the measured frequencies, masses and Dingle temperatures for $B<B_M$ is given in Table II. For $B>B_M$ (15 T$<B<$32 T), ten frequencies were detected, and with the possible exception of the Fermi surface branch at $F \approx 870$ T, none of the frequencies overlap with those measured below B_M. The dHvA data for $B>B_M$ is summarized in Table III. From this data, it is obvious that there is a major Fermi surface reconstruction at B_M as has been observed in other uranium systems such as UPt_3 and UPd_2Al_3 that display a metamagnetic transition.[40,41] As mentioned earlier, the transition in UGa_3 is unlikely metamagnetic where one expects a drastic change in the character of the f electron which manifests itself as an increase in the magnetization on the order of $1\mu_B$/U (we see an almost negligible change in the magnetization). From the measured

TABLE II. Measured de Haas–van Alphen frequencies F, effective masses m^*, and Dingle temperatures T_D for $B<B_M$ in UGa_3.

F (T)	m^* (m_e)	T_D (K)
885	1.9 ± 0.2	0.8
980	0.6 ± 0.1	2.9
1514	0.7 ± 0.2	2.0

TABLE III. Measured de Haas–van Alphen frequencies F, effective masses m^*, and Dingle temperatures T_D for $B > B_M$ in UGa_3.

F (T)	m^* (m_e)	T_D (K)
287	1.4±0.4	1.3
479	3.0±0.6	1.3
607	2.9±0.4	3.1
861	1.1±0.6	2.2
1367	4.0±1.5	0.3
1727	2.1±0.8	1.1
1929	0.8±0.4	1.8
2377	1.5±0.6	2.3
2512	5.0±1.4	0.8
2988	1.5±0.6	0.7

$C(T)$, we could not detect an anomaly which could be related to the transition at B_M observed in the magnetization and dHvA in fields to 12 T and temperatures down to 1.3 K.

The dHvA data for USn_3 and UAl_3 yield only a single frequency which can be seen in the FFT of the magnetization versus inverse field data for USn_3 and UAl_3 shown in Fig. 8. Though numerous peaks appear in the FFT for USn_3 in Fig. 8(a), after calculating the effective masses, all but the peak labeled with an asterisk at $F = 2080$ T have $m^* < 0.7 m_e$ and correspond to measured frequencies for elemental white Sn.[42] Because of this, we ascribe only the peak marked with an asterisk to be from USn_3, with the others coming from white Sn (this agrees well with the observation of Sn inclusions in our resistivity and magnetization measurements), and from the temperature dependence of the FFT amplitude, we estimate that $5 < m^*/m_e < 15$ for these carriers. As can be seen in Fig. 8(b), UAl_3 only shows a single weak peak at $F = 2510$ T. Due to the small amplitude of the dHvA oscillations in UAl_3, it is impossible to accurately determine the effective mass of the carriers, however, we can estimate that $1 < m^*/m_e < 4$.

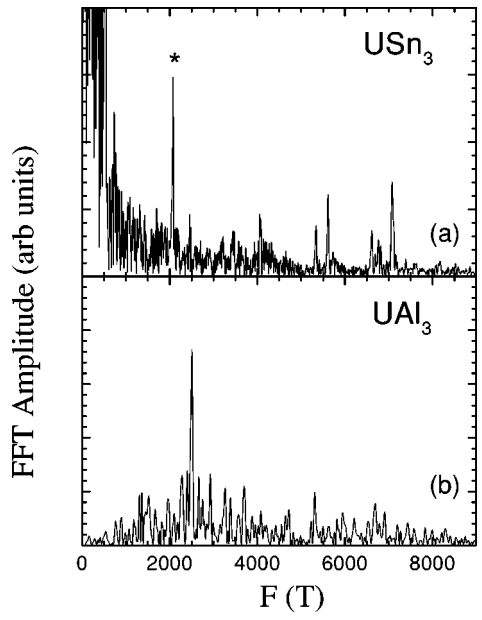

FIG. 8. The calculated fast Fourier transform of the de Haas–van Alphen data for USn_3 and UAl_3.

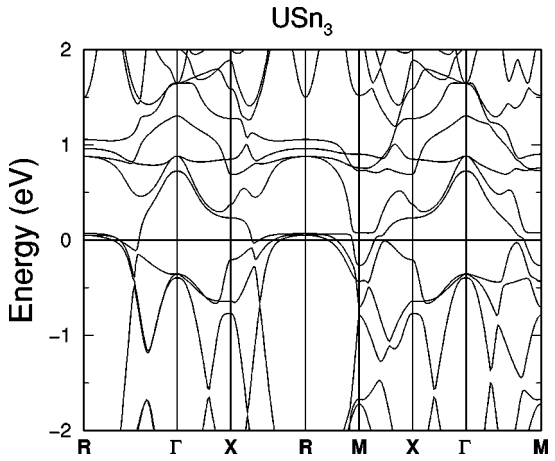

FIG. 9. The calculated band structure of paramagnetic USn_3. The results are similar to those of Strange (Ref. 41), except that we find only a single band crossing the Fermi energy (at 0 eV) in the X-M direction.

B. Band structure theory

Numerous band structure calculations have been made on the UX_3 compounds.[43–49] Our own calculations of the band structure of UAl_3, USn_3, and UGa_3 have been performed on the basis of density-functional theory in the local spin-density approximation (LSDA) (see, e.g., Ref. 50). This approach is appropriate for itinerant electrons. We have computed the energy band structure using a relativistic version of the augmented-spherical-wave (ASW) method.[51] Before we discuss our results, we mention that other calculations were previously performed for USn_3 and UAl_3.[43,49] Strange computed the Fermi surfaces of paramagnetic USn_3 in the simple cubic (sc) $AuCu_3$ structure,[43] and obtained five Fermi surface sheets. In general, the calculated Fermi surfaces tend to be closed. Along with our magnetoresistance measurements which do not tend towards saturation, it appears that USn_3, and also UAl_3, UGa_3, are compensated metals, though we need to do angle-resolved measurements of the magnetoresistance to say this with certainty. In our own calculations of the band structure of USn_3, shown in Fig. 9, we could confirm the results obtained by Strange, however, with the difference that the tiny Fermi surface sheet labeled δ-ϵ by Strange,[43] does not appear in our calculation. This tiny Fermi surface sheet corresponds to the energy band in the $M-X$ symmetry direction, which, in our calculation, falls just below E_F (see Fig. 9). A summary of the calculated Fermi surface parameters is given in Table IV. As mentioned, the

TABLE IV. The calculated Fermi surface parameters of USn_3 which contains two closed orbits around the R point, an M-centered ellipsoid with two extremal areas, and a piece in the middle of Γ-R (see Fig. 9 for band structure).

Orbit center	Fermi surface area (kT)	Band mass (m_e)
R	3.03	4.81
R	5.24	4.69
M	1.37	0.92
M	0.49	0.28
	1.27	1.70

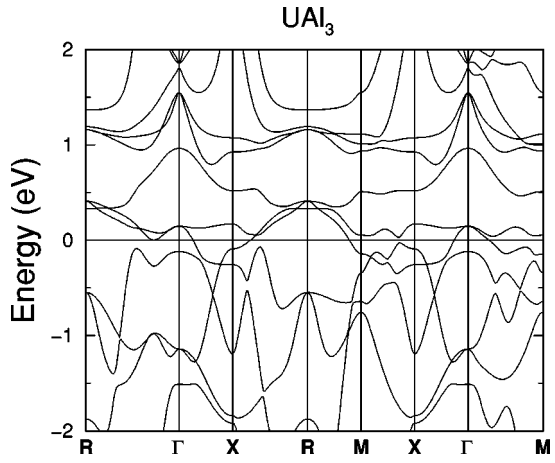

FIG. 10. The calculated band structure of paramagnetic UAl_3. There is only a single band that crosses the Fermi energy, that forms a closed orbit about the Γ point in the $z=0$ plane, and a large ''dogs bone'' orbit about the R point in the extended zone at $z=1/2$.

shape of the calculated Fermi surface is in good agreement with that of Strange[43] though there is a discrepancy in the calculated band masses. Our detection of a dHvA frequency of ~ 2 kT with a mass on the order of $5–15 m_e$ is consistent with the first or second R-centered orbit listed in Table IV. However, since band-structure theory predicts five extremal orbits, it remains to be solved why the other calculated dHvA frequencies have not been measured. It can, of course, be that the calculated LSDA bands at the Fermi energy do not straightforwardly correspond to the measured heavy quasiparticle bands. The latter arise from single-particle bands that are substantially renormalized by many-body interactions.

While the band structure of UAl_3 has been calculated,[49] the actual Fermi surface parameters have not been reported in the literature. We have computed the band structure of UAl_3, which we find to be quite different from a previous report.[49] Specifically, the latter band structure displays multiple bands crossing the Fermi level, e.g., four band crossings between X and M in the sc Brillouin zone.[49] The band structure we calculated is shown in Fig. 10. There is not a single band crossing between X and M. For the other symmetry directions similar differences occur. In our calculation there is altogether only one open Fermi surface sheet. (On the symmetry axis $R-\Gamma$ there is one band that is close to, but does not cross, E_F.) On this Fermi surface sheet there is one extremal orbit centered at the Γ-point in the $z=0$ plane, and also a large ''dogs bone'' type orbit in the extended zone scheme, centered at the R point. The calculated Fermi surface parameters are shown in Table V. The dogs bone orbit has a large Fermi surface area and a heavy mass, which

TABLE V. The calculated Fermi surface parameters of UAl_3. There is a single closed Γ-centered sheet and a large dogs bone R-centered orbit (see Fig. 10 for band structure).

Orbit center	Fermi surface area (kT)	Band mass (m_e)
Γ	1.74	1.64
R	14.08	5.24

makes its detection more difficult. The other, smaller extremal orbit on the Fermi surface sheet nicely coincides with the single dHvA oscillation we have detected for UAl_3 as both the frequency and mass measured by dHvA and determined from the band structure calculations are in good agreement. Although as yet the nature of the uranium $5f$ electrons of UAl_3 has not been thoroughly investigated, the agreement we have reached for the Fermi surface would advocate an itinerant nature of the $5f$ states. In the itinerant approach, the $5f$ electrons form a 2 eV wide band in the immediate vicinity of the Fermi energy (see Fig. 10). A localized description of the $5f$'s would remove the $5f$ states from the vicinity of E_F, leading thereby to a drastically changed Fermi surface. The calculated, unenhanced electronic specific heat coefficient $\gamma=16$ mJ/mol K^2 is a factor of 2.5 smaller than our experimental value. The elsewhere reported calculation,[49] however, yielded $\gamma=3.7$ mJ/mol K^2, a value deviating significantly from ours. A many-body enhancement factor of 2.5 is still acceptable for uranium compounds, so that we may conclude that the electronic specific heat coefficient, too, can be explained within an itinerant $5f$-electron model.

As mentioned before, UGa_3 has an antiferromagnetic ground state, where there are uranium moments aligned parallel in (111) planes which are coupled antiferromagnetically to the adjacent (111) planes.[18,19] The direction of the moments themselves is not known at present, though there are indications that the moments orient in the (001) direction.[20] We have investigated the ground state magnetic structure by performing total energy calculations for several magnetic arrangements, viz. the mentioned antiferromagnetic structure with the moments aligned in either the (001) or the (111) direction, two ferromagnetic structures with the moment aligned either along the (001) or the (111) axis, as well as paramagnetic UGa_3. Our calculations show that the considered antiferromagnetic arrangements have the lowest total energies, followed by the ferromagnetic structures, having energies higher by about 35 meV per formula unit (fu), in turn followed by the paramagnetic phase, being again higher in energy than the ferromagnetic phases by about 30 meV/fu. From a comparison of the total energies of the two antiferromagnetic structures we find that the one with the moments aligned in (001) direction has a 4 meV/fu lower total energy than the corresponding (111) direction. As a consequence, we obtain a ground state consisting of moments in antiferromagnetically coupled (111) planes, while the moments themselves are parallel to the (001) axis. This magnetic structure agrees with that inferred from experiments.[18–20] Our calculations reveal that the magnetic moments are unusually sensitive to both the magnetic structure and the lattice parameter. The f contribution to the uranium moment is $0.40\mu_B$ for the (001) antiferromagnetic orientation, but only $0.30\mu_B$ for the corresponding (111) structure, the spin part being about $1.65\mu_B$ in both cases. The two ferromagnetic structures display a similar behavior: the f contribution to the moment is close to $0.40\mu_B$ for the (001) orientation, but only $0.30\mu_B$ for the (111). However, for the ferromagnetic structures the spin and orbital contributions are quite different from those of the antiferromagnetic phases, only $1.39\mu_B$, $-1.78\mu_B$, respectively, for the (001) ferromagnetic phase. Thus, both are $0.26\mu_B$ smaller than the equivalent contributions to the

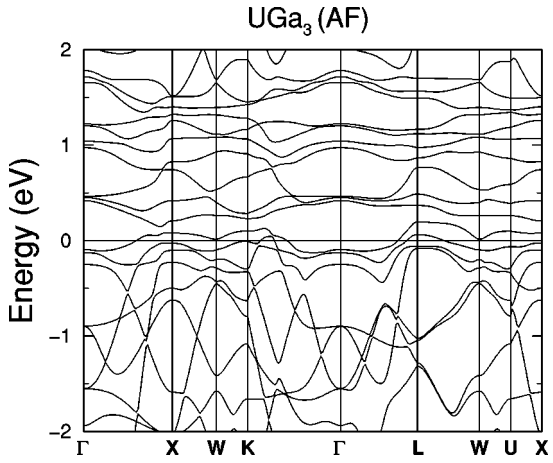

FIG. 11. The calculated band structure of UGa_3 in the antiferromagnetic (AF) state as discussed in the text.

moment for the (001) antiferromagnetic phase. The (111) ferromagnetic state has the same spin contribution as the (001) state, but the orbital part is reduced again by $0.10\mu_B$. These moments are calculated for the lattice constant $a = 4.248$ Å of Ref. 52, which is slightly smaller than the value of 4.260 Å we determined. Our calculated ground state uranium f moment of $0.40\mu_B$ is considerably smaller than the experimental one, which ranges from $0.82\mu_B$ (Ref. 14) to $0.95\mu_B$ in a more recent study.[18] In the present calculation we have not taken the so-called orbital polarization into account, which would increase the orbital moment.[54] But we wish to point out that a small expansion of the lattice parameter causes the moment to rise, which we find to be the case especially for the ferromagnetic state; e.g., a 0.7% larger lattice parameter yields already a 50% larger f moment of $0.60\mu_B$. The uranium moment thus depends critically on the magnetic structure and the lattice parameter, which is uncommon for uranium compounds. We consider this as clear evidence that UGa_3 is, rather atypical for uranium compounds, an itinerant antiferromagnet.

The unenhanced electronic specific heat, too, is calculated to be sensitive to the magnetic structure. In a previous study[17] it was reported that the experimental $\gamma = 52$ mJ/mol K^2 is reproduced by the calculated, unenhanced γ, taking a reasonable many-body enhancement factor of 2 into account. Also in the present calculations we obtain $\gamma = 26$ mJ/mol K^2 for the paramagnetic state and 25 mJ/mol K^2 for the (001) ferromagnetic state, but for the antiferromagnetic ground state a much smaller value of 12 to 16 mJ/mol K^2 (depending on the precise lattice parameter). The electronic contribution to γ of the antiferromagnetic state was not calculated previously, but in view of the fact that our calculation for the paramagnetic state reproduces the results of a previous calculation,[17] we consider the computed $\gamma = 12-16$ mJ/mol K^2 to be trustworthy. This indicates that there is a notable many-body enhancement factor of 3.3 to 4.3. The mechanism causing this many-body enhancement is currently unknown.

The calculated energy band structure of UGa_3 in the inferred antiferromagnetic structure with the moments in the (001) direction is shown in Fig. 11. Due to the antiferromagnetic order the number of atoms in the unit cell is doubled. We use therefore an fcc unit cell to describe this structure.

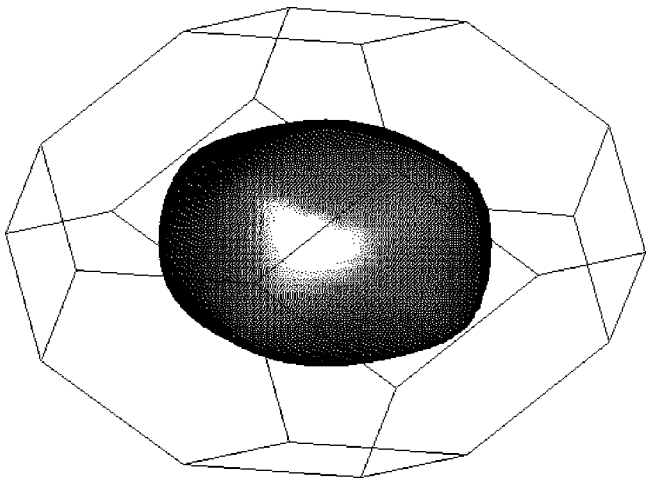

FIG. 12. A large Γ-centered rugby ball shape portion of the antiferromagnetic Fermi surface of UGa_3 shown in the reduced fcc Brillouin zone.

The flat bands visible in Fig. 11 in the energy range of -0.2 to 2 eV are the uranium $5f$ bands. Of these bands, two doubly degenerate bands are found to cross the Fermi energy. The Fermi surface sheets belonging to these two bands are shown in Fig. 12. There are, for the (001) direction, three branches: a large Γ-centered rugby-ball shaped sheet shown in Fig. 12, and the other two are extremal orbits on the entangled sheet shown in Fig. 13. One of the extremal orbits is located on the neck around the Z point, whereas the other one is located around the long axis of the bend ellipsoids in the $z = 0$ plane. The results of the Fermi surface calculation of antiferromagnetic UGa_3 are summarized in Table VI. The prediction of three extremal orbits is in agreement with our dHvA results where only three Fermi surface sheets are detected for $B < B_M$, and there is reasonable agreement between the masses determined by dHvA measurements and those in Table VI. The calculated dHvA frequencies, however, are not in a one-to-one correspondence to the measured frequencies. The dHvA frequency of the extremal orbit on the Γ-centered Fermi surface sheet is much larger than the three measured frequencies. The explanation for this could

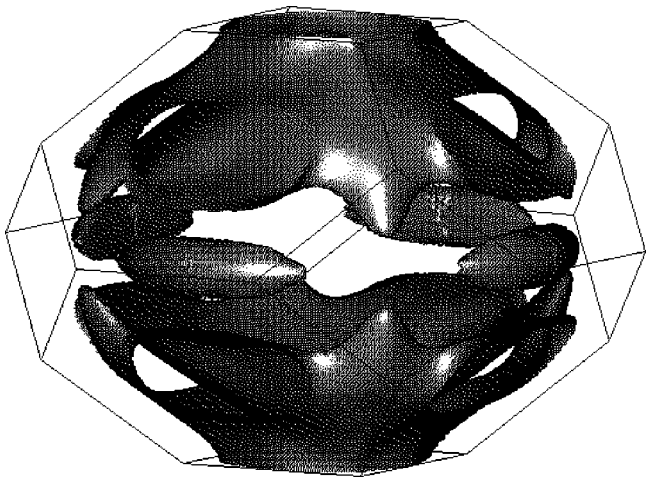

FIG. 13. Two pieces of the antiferromagnetic Fermi surface of UGa_3 are found on the shown entangled sheet displayed in the reduced fcc Brillouin zone.

TABLE VI. The calculated Fermi surface parameters of antiferromagnet UGa_3 (see Fig. 11 for band structure). There is a rugby ball shaped Γ-centered sheet shown in Fig. 12 and two extremal orbits on the entangled sheet, around the neck at the Z-point and on the ellipsoide, shown in Fig. 13.

Orbit center	Fermi surface area (kT)	Band mass (m_e)
Γ	6.28	1.83
Z	2.11	1.21
	0.52	0.65

again be the already mentioned unusual sensitive behavior of the magnetic moments, which occurs consequently also for the Fermi surfaces. Nevertheless, the fact that three extremal orbits are correctly predicted supplies, along with the measured specific heat γ, evidence for delocalized $5f$ behavior in UGa_3.

The nature of the magnetic transition taking place at $B_M \sim 12$ T is mysterious. One simple explanation which we examine here first is the transition to the (001) ferromagnetic state. This magnetic state yields a drastically different energy band structure as displayed in Fig. 14, where numerous intertwined band crossings can be seen. To facilitate comparison between the antiferromagnetic band structure in Fig. 11 and the ferromagnetic one, we displayed the ferromagnetic bands in the fcc unit cell also. The ferromagnetic state results in an extremely complicated Fermi surface, and it is unclear if we can even determine the number of extremal orbits. Once again, this seems in agreement with the dHvA results for $B > B_M$ where ten frequencies are observed. However, it is hard to believe that the transition at B_M is really to a ferromagnetic state, because, first, the calculated total energy difference of 35 meV/fu between the antiferromagnetic and ferromagnetic structure, is too large to be overcome by a field of 12 T, and, second, the fact that there is almost no anomaly in the measured magnetization curves and magnetoresistance at B_M. This would lead us to postulate that there is an, as yet unknown, change in the antiferromagnetic structure at B_M that causes the reconstruction of the Fermi surface. One of the clues to this reconstruction appears to be the

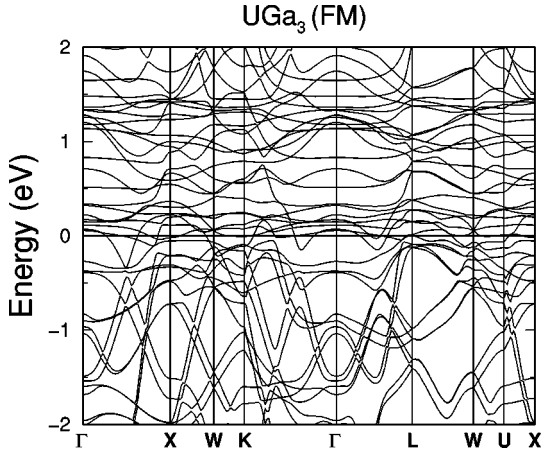

FIG. 14. The calculated band structure of UGa_3 in the ferromagnetic (FM) state with the moments in the (100) direction. For comparison to the antiferromagnetic band structure shown in Fig. 11, the energy bands are also shown in the fcc unit cell.

extreme sensitivity of the moments, and therefore of the energy bands at the Fermi energy, to the magnetic structure. For example, already the antiferromagnetic arrangement with the moments along the (111) axis yields a different Fermi surface with one more band crossing E_F. Thus, if some sort of buckling of the moments, or perhaps a spin-flop transition, takes place above B_M, it is quite reasonable to expect a concurrently modified Fermi surface. This is very different from most uranium compounds that have much more localized $5f$ electrons and, consequently, moments that remain rigid under rotation and small lattice parameter changes. While we currently do not know how precisely the magnetic structure is rearranged above B_M, we mention that very recently it has been observed on single crystals UGa_3 that two hitherto unknown singularities occur in the magnetic susceptibility at $T=8$ K and $T=40$ K, next to the already known singularity at the Néel temperature.[53] Investigations of the origin of these singularities and of the Fermi surface reconstruction will be continued. From our present results we conclude that it is evidently the itinerant nature of the $5f$ electrons that leads to a Fermi surface that can drastically be altered by the application of a magnetic field in contrast to most other uranium compounds.

IV. CONCLUSIONS

We have performed measurements of the specific heat and resistivity at zero field, specific heat measurements in static magnetic fields to 12 T and magnetic measurements in a static field of 5 T and pulsed fields to 50 T on the compounds UX_3 (X=Ga, Al, and Sn). The values of the electronic specific heat coefficients in applied fields $\gamma(B)$ behave differently for the three compounds with USn_3 increasing with increasing field and UGa_3 and UAl_3 remaining nearly constant.

The large variation of hybridization strengths of the $5f$ electrons with the conduction band electrons clearly manifests itself in the pronounced differences in the physical behavior of the UX_3 compounds. USn_3 is a heavy fermion compound, with a moderately enhanced specific heat coefficient. Although it is possible to fit the measured susceptibility to results[25] derived from the single-impurity (Coqblin-Schrieffer) model, the dependency of $\gamma(B)$ is in turn inconsistent with the single-impurity or Anderson lattice models. It is possible, however, that the $\gamma(B)$ results can be explained by a magnetic-field enhanced term to the specific heat that is not of a purely electronic origin. In the absence of this extra term not of electronic origin, only a metamagnetic transition in USn_3 occurring at fields higher than used in the current study would reconcile these contradicting observations. However, we could so far not detect a metamagnetic transition in fields up to 50 T and at $T \sim 0.5$ K. These results imply that USn_3 is better interpreted as a spin-fluctuation system. A single weak dHvA frequency could be observed which could correspond to the smaller orbit about the R point.

UAl_3 is a weakly temperature-dependent paramagnet. Only above 240 K does it display Curie-Weiss behavior. UAl_3 has previously been classified as a spin-fluctuation system,[12] and our specific heat measurements support this interpretation. We measured no discernible variation of $\gamma(B)$

at low temperature, which cannot be explained within the single-impurity or Anderson lattice models. The dHvA measurements showed a single, weak dHvA signal, which nicely corresponds to the result of our band structure calculation based on an itinerant $5f$-electron approach. We thus conclude that at least at low temperatures the uranium $5f$ electrons have a tendency towards delocalization.

UGa_3 is the only UX_3 compound considered to be itinerant that displays magnetic order. The other two itinerant UX_3 compounds, UGe_3 and URh_3, are paramagnetic and were found to have magnetic form factors similar to transition metal compounds[55] and Fermi surfaces determined from dHvA that agree with band structure calculations.[46] Also the dHvA signals observed for UGa_3 agree well with the result of band structure calculations assuming itinerant $5f$-electron behavior. A dramatic transformation of the Fermi surface of UGa_3 occurs at an applied field of $B_M \sim 12$ T at $T \sim 0.5$ K. UGa_3 exhibits obviously a Fermi surface that is very sensitive to magnetic structure and atomic volume making it unique among the UX_3 compounds. Our investigation lead us to conclude that the fact that UGa_3 is the only itinerant, magnetically ordered UX_3 compound explains the sensitivity of the Fermi surface to the application of a magnetic field. Increasing the field range of the dHvA measurements on UGe_3 and URh_3 may also prove to yield interesting results.

ACKNOWLEDGMENTS

Work at LANL was performed under the auspices of the U.S. Department of Energy, and the NHMHL is supported by the NSF and the state of Florida. We would like to thank R. Modler for assistance on the transport measurements. One of us (P.M.O.) thanks D. Kaczorowski for an informative discussion and A. Perlov for valuable assistance.

[1] J. M. Fournier and R. Troć, in *Handbook on the Physics and Chemistry of the Actinides* (North-Holland, Amsterdam, 1985), Vol. 2, Chap. 2, p. 29.
[2] H. H. Hill, in *Plutonium and Other Actinides*, edited by W. N. Miner (AIME, New York, 1970), p. 2.
[3] D. D. Koelling, B. D. Dunlap, and G. W. Crabtree, Phys. Rev. B **31**, 4966 (1985).
[4] H. R. Ott, F. Hulliger, H. Rudigier, and Z. Fisk, Phys. Rev. B **31**, 1329 (1985).
[5] M. H. van Maaren, H. J. van Daal, K. H. J. Buschow, and G. J. Schinkel, Solid State Commun. **14**, 145 (1974).
[6] A. Blaise, J. Phys. (France) **40**, 49 (1979).
[7] T. Moriya, *Spin-Fluctuations in Itinerant Electron Magnetism* (Springer, Berlin, 1985).
[8] S. D. Bader, G. S. Knapp, and H. V. Culbert, in *Magnetism and Magnetic Materials*, AIP Conf. Proc. No. 24, edited by C. D. Graham, G. H. Lander, and J. J. Rhyne (AIP, New York, 1975), p. 145.
[9] M. R. Norman, S. D. Bader, and H. A. Kierstead, Phys. Rev. B **33**, 8035 (1986).
[10] K. H. J. Buschow and H. J. van Daal, in *Magnetism and Magnetic Materials*, AIP Conf. Proc. No. 5, edited by D. C. Graham and J. J. Rhyne (AIP, New York, 1972), p. 1464.
[11] M. Loewenhaupt and C. K. Loong, Phys. Rev. B **41**, 9294 (1990); W. G. Marshall, A. P. Murani, and K. A. McEwan, J. Magn. Magn. Mater. **104-107**, 67 (1992).
[12] I. Lupsa, E. Burzo, and P. Lucaci, J. Magn. Magn. Mater. **157/158**, 696 (1996).
[13] P. C. Canfield and Z. Fisk, Philos. Mag. B **65**, 1117 (1992).
[14] A. Murasik, J. Leciejewicz, S. Ligenza, and A. Zygmunt, Phys. Status Solidi A **23**, K147 (1974).
[15] D. Kaczorowski, R. Troć, D. Badurski, A. Böhm, L. Shlyk, and F. Steglich, Phys. Rev. B **48**, 16 425 (1993).
[16] D. Kaczorowski, R. Hauser, and A. Czopnik, Physica B **230-232**, 35 (1997).
[17] G. E. Grechnev, A. Delin, O. Eriksson, B. Johansson, A. S. Panfilov, I. V. Svechkarev, and D. Kaczorowski, Acta Phys. Pol. A **92**, 331 (1997).
[18] A. C. Lawson, A. Williams, J. L. Smith, P. A. Seeger, J. A. Goldstone, J. A. O'Rourke, and Z. Fisk, J. Magn. Magn. Mater. **50**, 83 (1985).
[19] A. Kratzer, C. Schopf, G. M. Kalvius, H. H. Klauß, S. Zwirner, and J. C. Spirlet, Hyperfine Interact. **104**, 181 (1997).
[20] D. Kaczorowski (private communication).
[21] G. R. Stewart, Rev. Mod. Phys. **56**, 755 (1984).
[22] K. Kadowaki and S. B. Woods, Solid State Commun. **58**, 507 (1986).
[23] T. Takimoto and T. Moriya, Solid State Commun. **99**, 457 (1996).
[24] A. L. Giorgi, G. R. Stewart, M. S. Wire, and J. O. Willis, Phys. Rev. B **32**, 3010 (1985).
[25] V. T. Rajan, Phys. Rev. Lett. **51**, 308 (1983).
[26] B. Andraka, J. S. Kin, G. R. Stewart, and Z. Fisk, Phys. Rev. B **44**, 4371 (1991).
[27] K. Satoh, T. Fujita, Y. Maeno, Y. Onuki, T. Komatsubara, and T. Ohtsuka, Solid State Commun. **56**, 327 (1985).
[28] S. Sullow, B. Ludoph, G. J. Nieuwenhuys, A. A. Menovsky, and J. A. Mydosh, Physica B **223-224**, 208 (1996).
[29] D. M. Edwards and A. C. M. Green, Z. Phys. B **103**, 243 (1997).
[30] H. P. van der Meulen, A. de Visser, J. J. M. Franse, T. T. J. M. Berendschot, J. A. A. J. Perenboom, H. van Kempen, A. Lacerda, P. Lejay, and J. Flouquet, Phys. Rev. B **44**, 814 (1991).
[31] N. Harrison, P. Meeson, P.-A. Probst, and M. Springford, J. Phys.: Condens. Matter **5**, 7435 (1993).
[32] H. P. van der Meulen, Z. Tarnawski, A. de Visser, J. J. M. Franse, J. A. A. J. Perenboom, D. Althof, and H. van Kempen, Phys. Rev. B **41**, 9352 (1990).
[33] J. Spalek, P. Korbel, and W. Wojcik, Phys. Rev. B **56**, 971 (1997).
[34] M. Kontani, T. Nishioka, Y. Hamaguchi, H. Matsui, H. A. Katori, and T. Goto, J. Phys. Soc. Jpn. **63**, 3421 (1994).
[35] A. Mielke, E. W. Scheidt, J. J. Rieger, and G. R. Stewart, Phys. Rev. B **48**, 13 985 (1993).
[36] J. S. Kim, B. Andraka, G. Fraunberger, and G. R. Stewart, Phys. Rev. B **41**, 541 (1990).
[37] S. R. Julian, P. A. A. Teunissen, and S. A. J. Wiegers, Phys. Rev. B **46**, 9821 (1992).
[38] S. Chapman, M. Hunt, P. Meeson, P. H. P. Reinders, M. Springford, and M. Norman, J. Phys.: Condens. Matter **2**, 8123 (1990).

[39] H. Aoki, S. Uji, T. Terashima, M. Takashita, and Y. Ōnuki, Physica B **201**, 231 (1994).
[40] N. Kimura, R. Settai, Y. Onuki, K. Maezawa, H. Aoki, and H. Harima, Physica B **216**, 313 (1996).
[41] Y. Inada, H. Aona, A. Ishiguro, J. Kimura, N. Sato, A. Sawada, and T. Komatsubara, Physica B **119-200**, 119 (1994).
[42] W. A. Roger, J. A. Rowlands, and S. B. Woods, J. Phys. F **6**, 315 (1976).
[43] P. Strange, J. Phys. F **16**, 1515 (1986).
[44] A. J. Arko and D. D. Koelling, Phys. Rev. B **17**, 3104 (1978).
[45] A. J. Arkow, M. B. Brodsky, G. W. Crabtree, D. Karim, D. D. Koelling, and L. R. Windmiller, Phys. Rev. B **12**, 4102 (1975).
[46] A. J. Arko, D. D. Koelling, and J. E. Schirber, in *Handbook on the Physics and Chemistry of the Actinides*, edited by A. J. Freeman and G. H. Lander (North-Holland, Amsterdam, 1985), Vol. 2, Chap. 3, p. 175.
[47] M. Divis, Phys. Status Solidi B **182**, K15 (1994).
[48] M. S. S. Brooks (unpublished).
[49] N. V. Chandra Shekar, P. C. Sahu, M. Rajagopalan, M. Yousuf, and K. G. Rajan, J. Phys.: Condens. Matter **9**, 5867 (1997).
[50] *Theory of the Inhomogeneous Electron Gas*, edited by S. Lundqvist and N. H. March (Plenum, New York, 1983).
[51] A. R. Williams, J. Kübler, and C. D. Gelatt, Phys. Rev. B **19**, 6094 (1979).
[52] J. M. Lawrence, M. L. den Boer, R. D. Parks, and J. L. Smith, Phys. Rev. B **29**, 568 (1984).
[53] D. Kaczorowski, P. W. Klamut, A. Czopnik, and A. Jezowski, J. Magn. Magn. Mater. **177-181**, 41 (1998).
[54] O. Eriksson, M. S. S. Brooks, and B. Johansson, Phys. Rev. B **50**, 9226 (1990).
[55] J. Trygg, J. Wills, B. Johansson, and O. Eriksson, Phys. Rev. B **50**, 9226 (1994).